2018

A Wheeled Robot Driven by a Liquid-Metal Droplet

Jian Wu
University of Science and Technology of China

Shiyang Tang
University of Wollongong, shiyang@uow.edu.au

Tao Fang
University of Science and Technology of China

Weihua Li
University of Wollongong, weihuali@uow.edu.au

Xiangpeng Li
Soochow University

See next page for additional authors

A Wheeled Robot Driven by a Liquid-Metal Droplet

Abstract

The controlled actuation of gallium liquid-metal (LM) alloys has presented new and exciting opportunities for constructing mobile robots with structural flexibility. However, the locomotion of current LM-based actuators often relies on inducing a gradient of interfacial tension on the LM surface within electrolytes, which limits their application outside a liquid environment. In this work, a wheeled robot using a LM droplet as the core of the driving system is developed that enables it to move outside liquid environment. The LM droplet inside the robot is actuated using a voltage to alter the robot's center of gravity, which in turn generates a rolling torque and induces continuous locomotion at a steady speed. A series of experiments is carried out to examine the robot's performance and then to develop a dynamic model using the Lagrange method to understand the locomotion. An untethered and self-powered wheeled robot that utilizes mini-lithium-batteries is also demonstrated. This study is envisaged to have the potential to expand current research on LM-based actuators to realize future complex robotic systems.

Publication Details

Wu, J., Tang, S., Fang, T., Li, W., Li, X. & Zhang, S. (2018). A Wheeled Robot Driven by a Liquid-Metal Droplet. Advanced Materials, 30 (51), 1805039-1-1805039-7.

Authors

Jian Wu, Shiyang Tang, Tao Fang, Weihua Li, Xiangpeng Li, and Shiwu Zhang

DOI: 10.1002/
Article type: Communication

Title: Wheeled Robot Driven by Liquid Metal Droplet

Jian Wu, Shi-Yang Tang, Tao Fang, Weihua Li, Xiangpeng Li*, Shiwu Zhang**

J. Wu, T. Fang, Prof. S. Zhang
Department of Precision Machinery and Precision Instrumentation, University of Science and Technology of China, Hefei, Anhui 230027, China
E-mail: swzhang@ustc.edu.cn

Dr. S.-Y. Tang, Prof. W. Li

School of Mechanical, Materials, Mechatronic and Biomedical Engineering, University of Wollongong, Australia
E-mail: shiyang@uow.edu.au

Prof. X. Li

The Robotics and Microsystems Center, College of Mechanical and Electrical Engineering, Soochow University, Suzhou 215006, China

E-mail: licool@suda.edu.cn

Keywords: Liquid metal; untethered robot; locomotion; EGaIn

Abstract

Controlled actuation of gallium liquid metal alloys has presented new and exciting opportunities for constructing mobile robot with structural flexibility. However, locomotion of current liquid metal-based actuators often relies on inducing a gradient of interfacial tension on the liquid metal surface within electrolytes, limiting their applications outside liquid environment. In this work, we develop a wheeled robot using a liquid metal droplet as the core of the driving system for enabling the locomotion of the robot outside liquid environment. We actuate the liquid metal droplet within the robot using a voltage to alter the robot's center of gravity for generating a rolling torque and therefore, inducing continuous locomotion of the robot at a steady speed. We conduct a series of experiments to explore the motion performance of the robot, and we develop a dynamic model using Lagrange method to understand the behavior of the locomotion. Furthermore, we successfully demonstrate an untethered and self-powered wheeled robot utilizing mini lithium batteries. Thus, we envisage that this study has the potential to expand current research on liquid metal-based actuators to realize future complex robotic systems.

Some animals and plants smartly adopt wheeled mechanisms that exploit rotary mechanics for realizing continuous locomotion[1]. For example, some caterpillars can curl into a wheel and generate a rolling momentum to escape; and tumbleweed can detach from its root or stem, tumbling away in the wind once it is mature and dry. Inspired by our nature, researchers have developed various rolling robots that mimic the animals/plants rolling movements to interact with their environments[2]. The design of most rolling robots is based on the principle of altering their center of gravity (CG) to induce a rolling momentum that causes a wheel or sphere to roll[3]. Robots based on the rolling locomotion have relatively high velocity and flexibility, with simple and compact structures that can readily alter their moving direction[4]. Various actuators have been demonstrated for altering the CG of the rolling robots, such as motors, shape memory alloys, and pneumatic actuators[5].

Gallium-based liquid metal (LM) alloys, such as eutectic gallium indium (EGaIn, m.pt. 15.5 °C) and gallium indium tin (Galinstan, m.pt. −19 °C), is increasingly attracting researchers' attention in recent years. Harnessing the unique physical/chemical properties of the liquid metals, such as high thermal/electrical conductivities, favorable flexibility, and capable of forming a thin oxide shell when expose to oxygen[6], many applications have been explored deriving from these properties, including making chip cooling systems[7], forming 3D structures[8], fabricating flexible electronic components[9], as well as producing 2D nanomaterials[9b,9c]. Moreover, liquid metal droplets have drawn attentions for forming innovative actuators since they can be manipulated using various methods adopting electrical, magnetic, chemical and optical machenisms[10], making them useful in microfluidics[11] and robotics[12]. However, coating or mixing the LM with other materials such as ferromagnetic microparticles, catalyst, or aluminum strips, is generally required for actuating LM droplets using magnetic, optical or chemical methods. This may significantly affect the intrinsic properties and compromise the liquidity of the LM. Alternatively, actuating LM droplets using electrical approach can obtain a high locomotion velocity with the minimum effect on the properties of LM. This is achieved by inducing an interfacial tension gradient along the surface of LM droplet with the application of exterior electric fields[13]. Nonetheless,

previous studies show that robotic systems driven by such a locomotion method can only be achieved within a solution[13-14], and this greatly limits the scope of integrating LM as the core of the actuator for forming a more complex system. Therefore, we have been impelled to investigate an innovative method that can harness the actuation of LM droplets to enable the locomotion of a more complex robotic system outside liquid environment.

Here, we report the design and investigation of a wheeled robot containing an EGaIn LM droplet and electrolyte within an enclosed system, and such an enclosed system is used as the core of the driving module for enabling the locomotion of the robot outside liquid environment. The LM droplet-powered driving module is controlled using a pair of electrodes. When applying a voltage to the electrodes, the confined LM droplet can be actuated within an electrolyte and consequently, alters the CG of the wheeled robot and continuously drives the wheel to roll at a steady speed. This implies that the robot can actuate in an environment outside a solution. We conducted a series of experiments to explore the parameters affecting the locomotion performance of the wheeled robot, such as the diameter of the wheel, the voltage on the electrode, the volume of the LM droplet, and the concentration of the electrolyte. We also developed a Lagrangian dynamic model to understand the actuating mechanism and explain the locomotion behaviors of the wheeled robot. Finally, we demonstrated a self-powered and fully untethered wheeled robot system carrying a mini cylindrical lithium battery as the power source, and we found that the robot could successfully roll on a flat surface at an angular velocity up to 1.8 rad/s. Our study certainly possesses the potential to significantly broaden the applications of LM in robotic systems.

Design of the wheeled robot. The wheeled robot consists of two major parts - the wheel body and the driving module, as shown in **Fig. 1**a. The driving module consists of a LM droplet that is surrounded by sodium hydroxide (NaOH) solution, and the droplet is driven by an electrode module that is connected to an external power source through two fine enameled wires, as shown in Fig. 1b. The wheel body is made of thin polymethyl methacrylate (PMMA) sheets (200 μm), and the surface of the PMMA is chemically treated to make it superydrophobic (contact angle of a water droplet is >150º), the detailed manufacturing process is given in Supplementary Fig. S1. The bracket of the electrode module is 3D printed and the electrodes are fixed at the both ends of the bracket (Fig. 1b). The electrode module lies on the inner flanges of the wheel body supported by the sleeves. A LM droplet and NaOH solution are injected between the two electrodes by a pipette. The wheel flanges confine the LM droplet to form a long worm-shaped slug. The semi-closed design of the wheel body avoids the accumulation of gas from electrolysis, and enables the movement of the driving module in the wheel. More details of the robot are shown in Supplementary Fig. S2.

The driving module and its working mechanism are depicted in Fig. 1c. Upon the application of a potential to the electrodes, a driving force, *F*, can be produced on the LM droplet to drive it towards the cathode (Fig. 1c)[14a]. Correspondingly, the LM droplet moves inside the wheel channel, and push the electrode module along the wheel flanges. The distance between the two electrodes are carefully adjusted to avoid the contact with the LM droplet. During the steady speed locomotion, the driving force exerted on the LM droplet is balanced by the resistive forces including the viscous resistance between the droplet and the surrounding NaOH solution, the friction between the LM droplet and the wheel, as well as the friction between the electrode module and the flanges of the wheel (Fig. 1c). We observed that the LM droplet actuate towards the cathode. Such a cathode-oriented locomotion is probably due to the bipolarization of the elliptical-shaped LM droplet within the confined channel, and the formation of a gallium oxide layer on the anodic pole of the droplet significantly lowers its interfacial tension[15]. Consequently, the induced Marangoni flow from the area with a lower interfacial

tension (anodic pole) drives the LM droplet towards the cathode instead of the anode, which is different from our previously reported results on spherical-shaped LM droplet without bipolarization[13]. The superhydrophobic coating on the internal surface of wheel body decreases the viscous resistance. Meanwhile, the Teflon tube sleeves on the four axes of the electrode module reduce frictional forces between the module and the flanges of the wheel. Fig. 1d shows the rolling locomotion of an actual wheeled robot (with a radius of 25 mm) driven by a 0.7 mL LM droplet merged within 500 μL 2 M NaOH solution; the LM droplet was activated using a 15 V DC voltage (also see Supplementary Movie S1). A rolling speed of 5.5 cm/s was obtained, and the time-displacement plot (inset of Fig. 1d) of the wheeled robot indicates that the wheeled robot can roll with a steady speed at a steady angular velocity ω (2.2 rad/s).

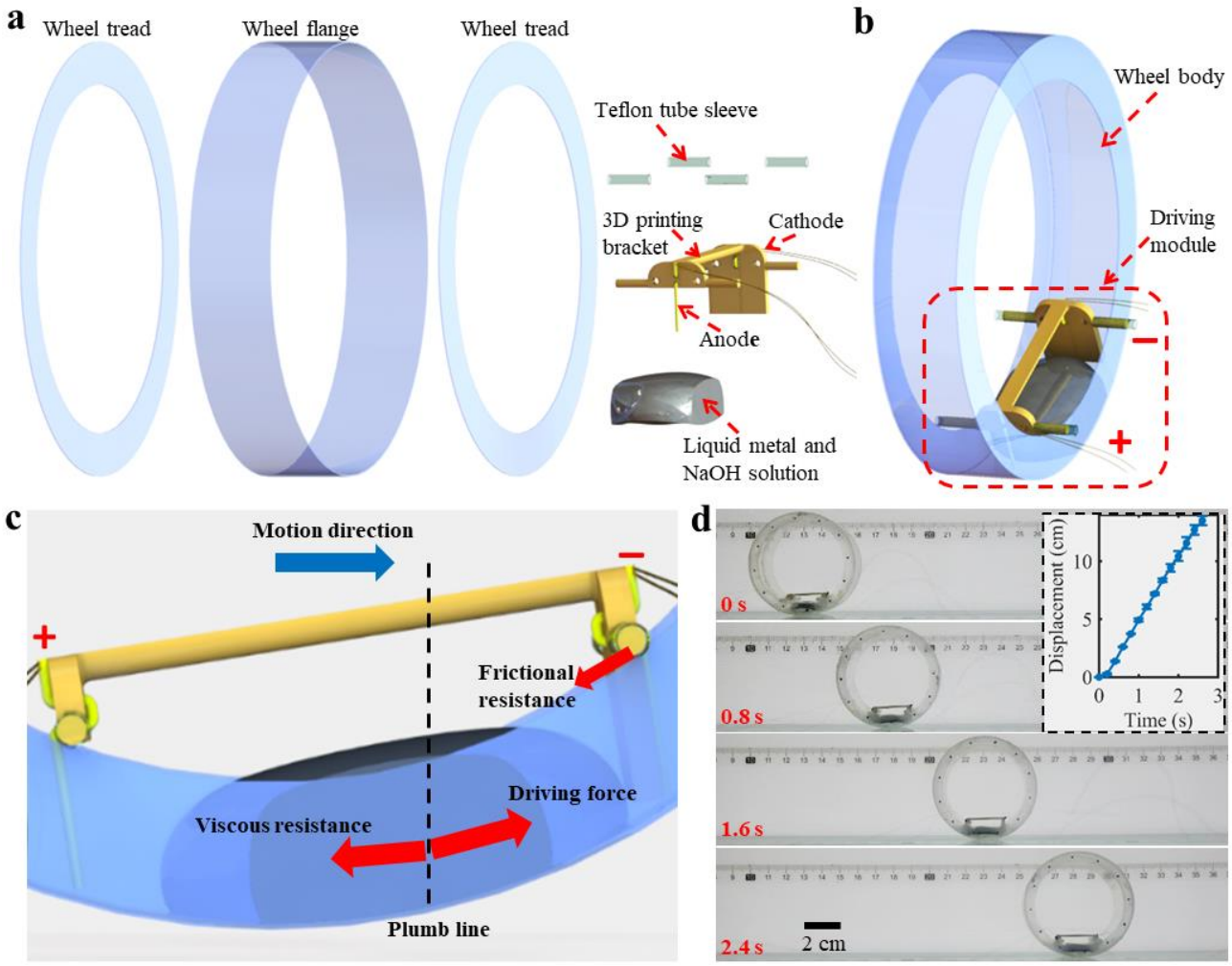

Figure 1. Working mechanism of the wheeled robot. (a) Explosive view and **(b)** 3D view of the wheeled robot powered by an external power source. **(c)** Schematic of the driving module and the working mechanism. **(d)** Sequential snapshots for the actuation of an actual wheeled robot at a steady speed, the inset shows the time-displacement plot.

Characterization of the actuating performance. We conducted a series of experiments to examine the motion characteristics of the LM actuated wheel. We found that there are four main factors affect the locomotion performance of wheeled robot, including *1)* the concentration of the NaOH solution C; *2)* the supplying voltage U; *3)* the volume of liquid metal V_{LM}; and *4)* the radius of wheel R. Based on the principle of control variables, we have carried out a series of experiments to explore the influence

of these four factors. The locomotion performance of the robot is characterized by recording the rolling speed ω and the power consumption P. **Fig. 2**a displays the ω and P of the wheeled robot with respect to different concentrations C. We can see that ω increases until C reaches 2 M, and the ω decreases despite the increased P at a higher C. Within a 2 M NaOH solution, we investigated the influence of U on the locomotion performance of the wheeled robot, as given in Fig. 2b. The wheel cannot be actuated when U is less than 7 V, and ω increases until U reaches 15 V. However, ω of the wheeled robot remains unchanged when the voltage is above 15 V. From this experiment, we can conclude that the optimal operating voltage is 15 V.

Different volume of liquid metal droplets V_{LM} and radius R of the wheels will also affect the locomotion performance. Here, we operate the robot using a NaOH solution with the concentration of 2 M, and apply a 15 V supplying voltage for the experiment. With the increased V_{LM}, both ω and P increases and reaches there maxima when V_{LM} is 0.7 mL, as shown in Fig. 2c. We observed the decrease of both ω and P when using a larger LM droplet. For different R, we found that the robot with an R of 22.5 mm exhibits a better locomotion performance than the robots with an R of 20, 25, and 27.5 mm in most cases (Fig. 2d). At the optimum operating parameters of R = 22.5 mm, C = 2 M, V_{LM} = 0.7 mL, and U = 15 V, a maximum ω of 2.5 rad/s can be obtained. We also monitored the change of pH for the NaOH solution due to electrolysis during the experiment. Since we only used a small amount of NaOH solution (C = 2 M) to operate the robot, we diluted the solution by 100 times so that a bench pH meter can be used for the measurement. The pH of the diluted NaOH solution is ~12.04 before electrolysis, and we found that no obvious change of pH could be detected until we operate the wheeled robot for 3 min, which the pH gradually increased to ~12.16.

We found that if the volume of LM droplet is too small (< 0.4 mL), the droplet will be in spherical shape due to its large surface tension, also the droplet will actuate towards the anode. However, the change of the CG is insignificant since the LM droplet is small and therefore, the induced actuation force is not sufficient to produce enough rolling torque on the wheeled robot, as shown in

Supplementary Fig. S3. On the contrary, if the volume of the LM is too large (> 1.2 mL), the droplet will exceed the height of the flanges on both sides of the wheel, and the NaOH solution can spill out of the wheel and hinder the movement of the wheel, as shown in Supplementary Fig. S4. For the wheels with different diameters, there exists a reasonable range for the volume of LM droplet.

The influence of R on the motion performance of the wheel is rather a complicated problem. Usually, for a LM droplet with a constant V_{LM}, a wheel with a larger R means a larger frictional force needs to be overcome during the rolling process. However, if R is too small, the friction between the sleeves and the flanges becomes larger due to the increased contact angle, and the rolling speed will decrease correspondingly. Therefore, our experiments show that a wheel with an R of 22.5 mm is able to provide the optimum performance.

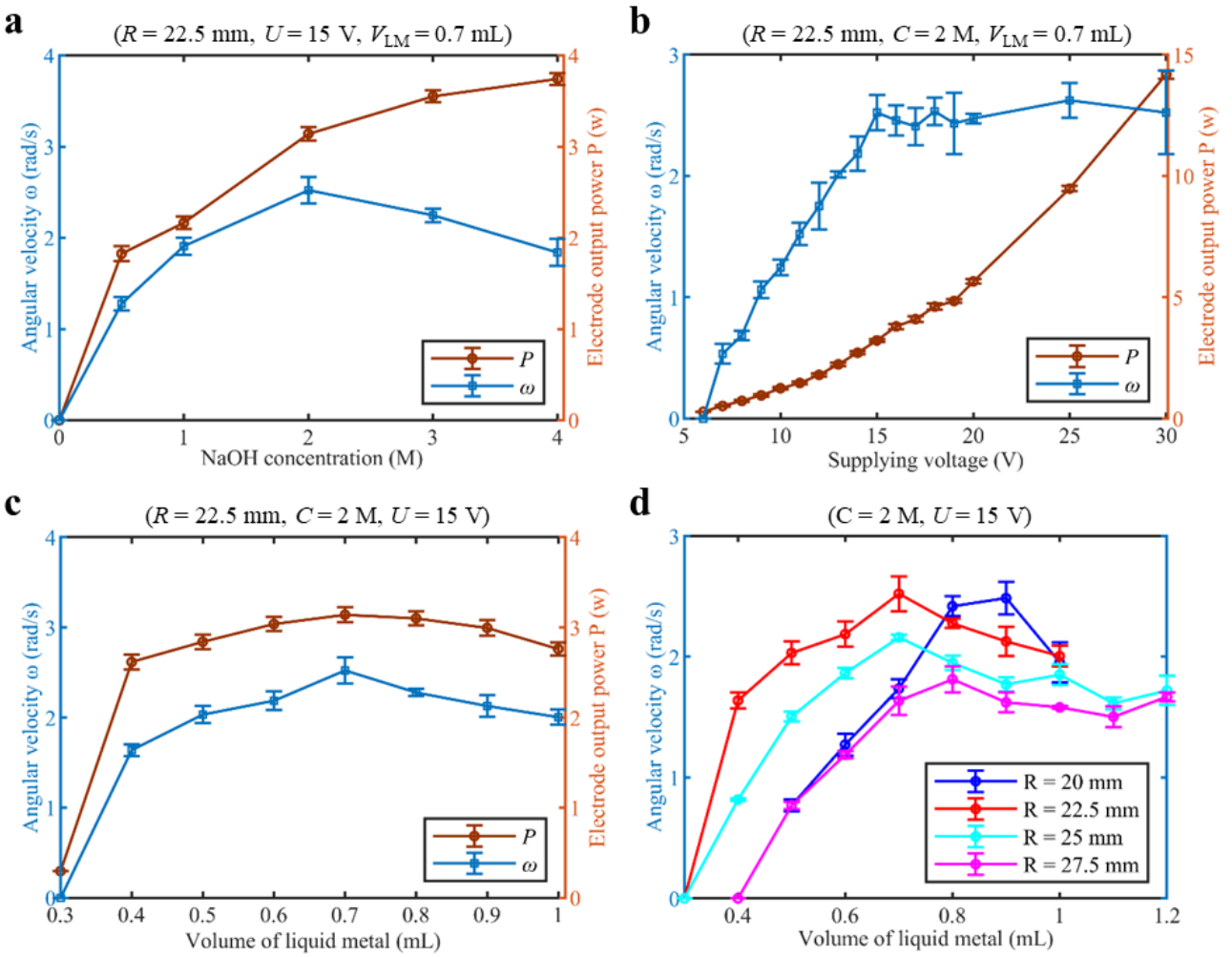

Figure 2. Characterization of the locomotion performance with respect to different operating parameters. (a) The influence of the concentration of the NaOH solution *C*. **(b)** The influence of the supplying voltage *U*. **(c)** The influence of the volume of liquid metal V_{LM}. **(d)** The influence of the radius of the wheel and the volume of liquid metal *R*.

Dynamic analysis of the wheeled robot. In order to have a better understanding on the locomotion performance of the wheeled robot, we derived a dynamic model for the rolling motion of the wheeled robot on a flat surface based on Lagrangian method, as shown in **Fig. 3**a. The moving direction is towards the x-axis. After ignoring the drag induced by air and the frictional resistance between the robot and the floor, the whole system can be equivalent to two parts: *1)* the wheel body with the weight of m_s, radius of *R* and rotational inertia of I_s; and *2)* the driving module with the weight of m_m. Before

applying an external potential, the wheeled robot is static on the flat surface at the contact point *A*. Once activating the robot, a driving force *F* is exerted on the LM droplet towards the cathode, the force would push the driving module to move along the flanges of the wheel, and the wheeled robot begins to roll due to the unbalanced CG. After a period of Δt, point *A* reaches a new position and the wheel body rotates θ degree, while the driving module rotates α degree. Combining Lagrange equation (see Supplementary Tab. 1), we can obtain the linear rolling equation of the wheeled robot as follow:

$$M\ddot{q} + C_{\mathrm{LM}}\dot{q} + H = Q \tag{1}$$

where

$$M = \begin{bmatrix} I_s + m_s R^2 + m_m R^2 + m_m r^2 - 2m_m Rr\cos(\alpha-\theta) & -m_m r^2 + m_m Rr\cos(\alpha-\theta) \\ m_m Rr\cos(\alpha-\theta) - m_m r^2 & m_m r^2 \end{bmatrix},$$

$$q = \begin{bmatrix} \theta \\ \alpha \end{bmatrix},\ C_{\mathrm{LM}} = \begin{bmatrix} m_m Rr\left(\dot{\alpha}-\dot{\theta}\right)\sin(\alpha-\theta) + \xi_s & m_m Rr\left(\dot{\theta}-\dot{\alpha}\right)\sin(\alpha-\theta) \\ 0 & \xi_m \end{bmatrix},$$

$$H = m_{\mathrm{m}} grs\begin{bmatrix} -1 \\ 1 \end{bmatrix},\ Q = \begin{bmatrix} 0 \\ Fr \end{bmatrix}$$

ξ_s/ξ_m denotes the viscous friction coefficient between the wheel body/LM droplet and the surrounding electrolyte. The exerting point of the driving force locates at the CG of the LM droplet, and the distance between the CG of the LM droplet's and the wheel's center $r = R–h/2$ (see Fig. 3a), *where h* is the height of the LM droplet.

From our experimental results, we found that the locomotion of the wheeled robot could be mainly separated into two stages: the accelerating stage and steady rolling stage. Once we activate the electrodes, the liquid metal droplet inside the wheel is elongated firstly (0-200 ms) and rapidly pushes the wheel to roll at a steady speed in less than 400 ms, as shown in Fig. 3b, (also see Supplementary Movie S2). In other words, the wheeled robot starts at a high angular acceleration, and reaches a steady speed in a very short amount of time. The dynamics of the rolling angle, rolling angular velocity and rolling angular acceleration in the experiment are in good agreement with those from the simulation

results according to our dynamic model, as shown in Fig. 3c (the parameters used for the simulation are given in Supplementary Tab. 2).

When the locomotion process becomes stable, the LM droplet deviates from the vertical line at a constant angle of β_0. Combining the linear rolling Equation (1), we can calculate the angular velocity ω of the wheel at the stable rolling stage from the following Equation.

$$\omega = \frac{F \cdot r}{\xi_s + \xi_m} \tag{2}$$

From the equation , we can see that ω of the wheel is positively correlated with the driving force of liquid metal F and the distance of r; also ω is negatively correlated with the sum of the viscous friction coefficient $\xi_s + \xi_m$.

From the actual experimental data given in Fig. 2, as the voltage U, the concentration C and the volume V_{LM} increase, the bipolarization effect is becoming more significant and the driving force F increases at first before reaching its saturation point. However, with the increase of C and V_{LM}, the viscous friction coefficient will also increase. Using Equation (2) we can explain the saturation trend observed between ω and U (Fig. 2a), as well as between ω and C (Fig. 2b). Meanwhile, with the increase of U and C, the electrolysis of the NaOH solution also enhances, thus, the power consumption of the system also increases (Figs. 2a and b).

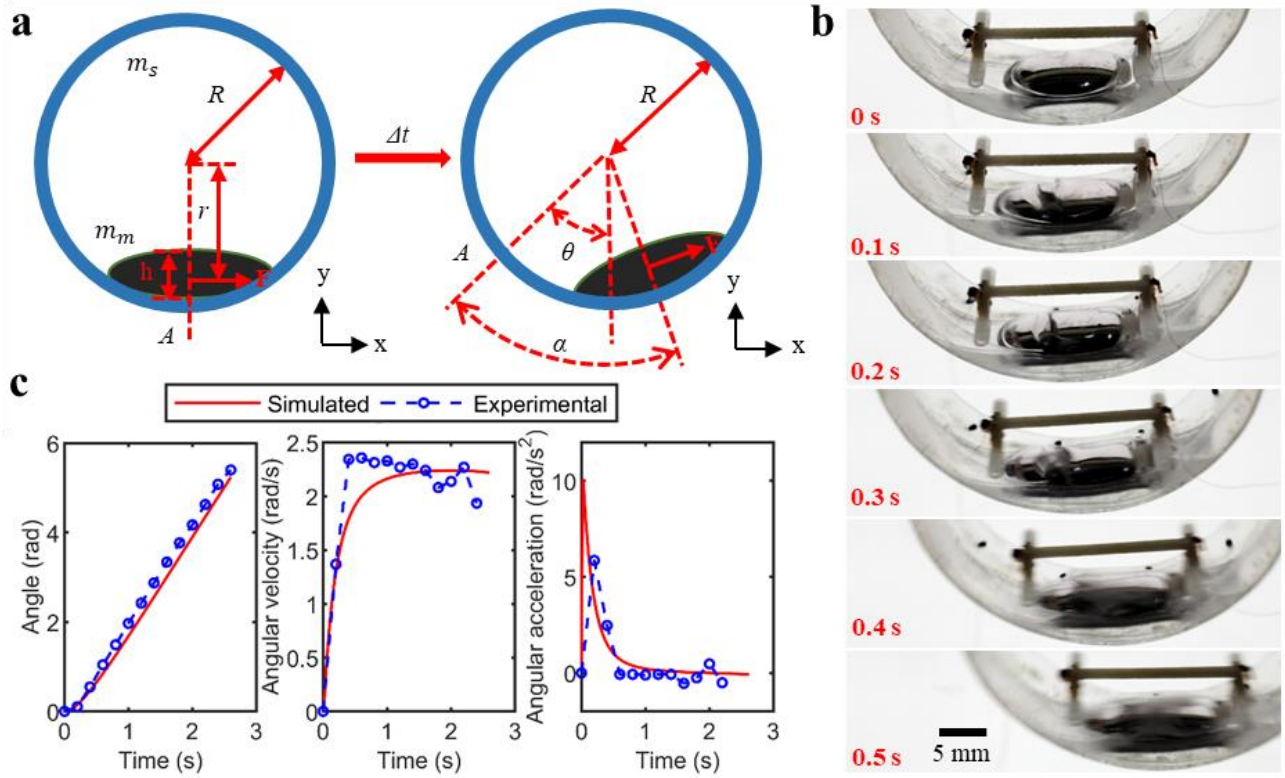

Figure 3. Dynamic model for the locomotion process of the wheeled robot. (a) Dynamic model of the wheel powered by an external power source moving on a flat surface. **(b)** Sequential snapshots of the wheeled robot during the locomotion process. **(c)** Dynamic of the rolling angle, rolling angular velocity, and rolling angular acceleration during the locomotion process from the simulation and experimental results (R = 25 mm, C = 2 M, U = 15 V, V_{LM} = 0.7 mL).

Developing an untethered and self-powered wheeled robot. After understanding the working mechanisms and the operating performance of the wheeled robot, we designed and manufactured an untethered wheeled robot that carries a series of mini cylindrical lithium batteries operated under the optimum parameters obtained from our experiments, the structure of the self-powered wheeled robot is given in **Fig. 4**a. We added two scaffolds onto the both sides of the wheel flanges so that the center of the wheel could support the battery, and the addition of the scaffolds does not affect the movement of the electrode module. Four mini lithium batteries were connected in series and placed in the shaft

of the scaffolds. The batteries together can provide a 16 V voltage, and the capacity of each battery is 55 mAh. The total mass of the self-powered robot is ~11.27 g, and the mass of each component is given in Supplementary Tab. 3. We found that the untethered wheeled robot is able to move smoothly after switching on the power, reaching a steady angular velocity of 1.8 rad/s, as demonstrated in Fig. 4b (also see Supplementary Movie S3). The relationship between the displacement and the time is presented in the inset of Fig. 4b.

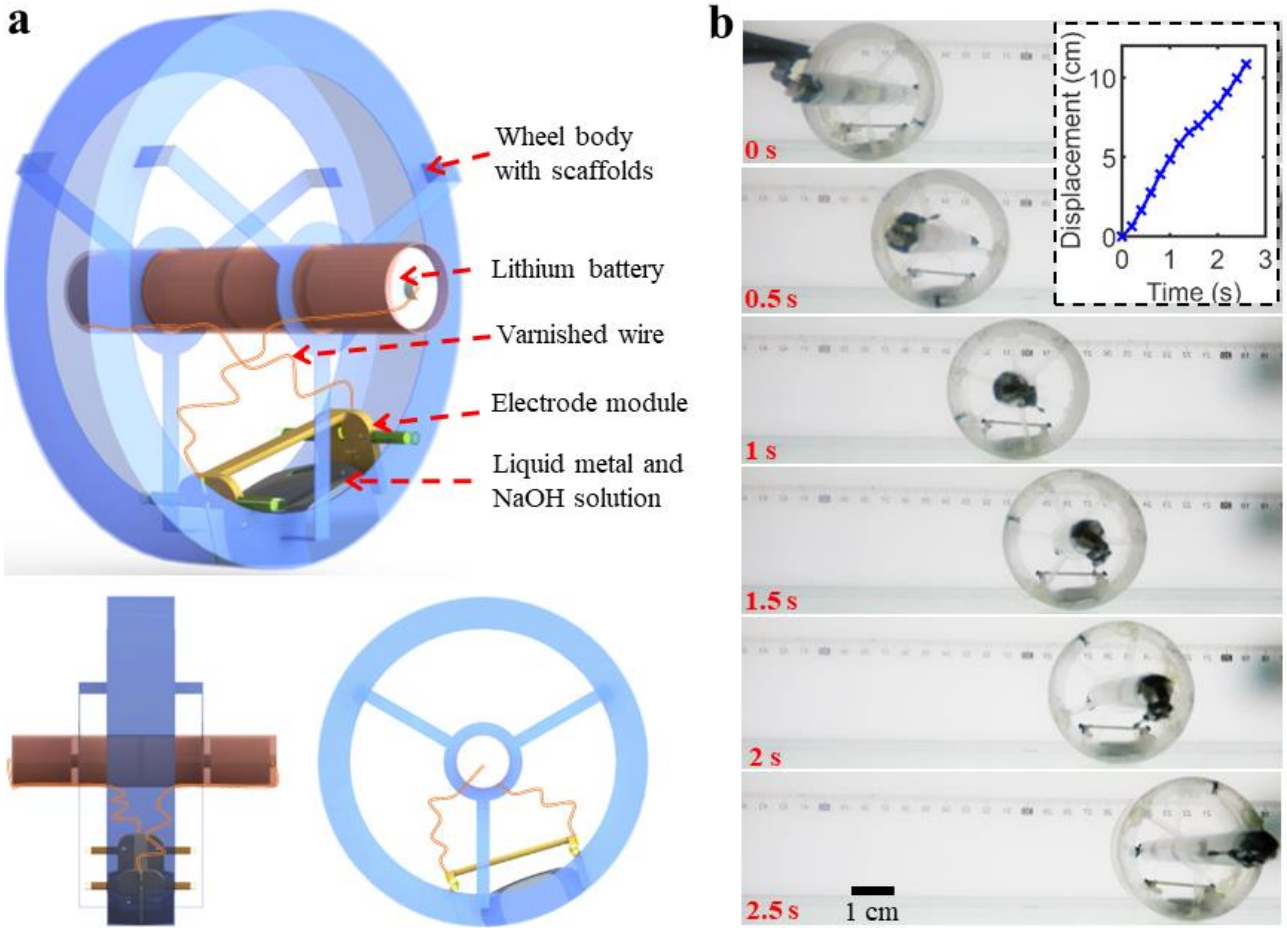

Figure 4. Demonstration of an untethered and self-powered wheeled robot driven by liquid metal droplet. **(a)** Structural design of the wheeled robot (R = 22.5 mm, C = 2 M, V = 0.7 mL, U = 16 V). **(b)** Sequential snapshots and time-displacement plot for the untethered wheeled robot.

In summary, we demonstrated the development of a wheeled robot driven by an EGaIn LM droplet. The controlled movement of the LM droplet is able alter the CG of the wheeled robot and induce the rolling locomotion outside liquid environment. We found that the wheeled robot is able to actuate at a relatively steady speed, reaching a maximum angular velocity of 2.5 rad/s. We explored the effects of different structural and operating parameters on the locomotion performance of the robot, and obtained the optimum radius of wheel, volume of LM droplet, supplying voltage, and concentration of NaOH solution for achieving the maximum speed with relative low power consumption. We also established a dynamic model to analyze the actuating behavior of the robot, and our model matches the actual experimental results. Moreover, taking the advantage of our systems, we designed and manufactured an untethered wheeled robot self-powered by integrated lithium batteries that can actuate on a flat surface with an angular velocity of 1.8 rad/s. In comparison with other small-size rolling systems[16] (see Supplementary Tab. 4 for details), our liquid metal-driven wheeled robot is extremely simple and robust with excellent ability to maintain the consistency of motion. More importantly, unlike traditional complex driving components using motors or shape memory alloy, the driving module in this robot can be lightweight structured, untethered, and readily replaced due to the absence of delicate moving parts. As such, we believe this innovative study has the potential to enlighten the development of future complex liquid metal-enabled robotic systems.

Experimental Section

Materials and methods: In our experiments, EGaIn (75% Ga, 25% In) liquid metal is particularly exploited. All experiments were performed on a 120×500 mm glass plate, a camera (GOPRO frame rate of 60 fps) was placed in front of the wheeled robot to record the movement. The instant and the steady rolling speeds can be obtained by analyzing the series snapshot during locomotion. A programmable DC power supply (RIGOL DP800) was used to drive the liquid metal droplet. We kept

the supplying voltage constant during each locomotion experiment; a multimeter was applied to measure the voltage and current. We also calculated the power consumption during the rolling locomotion. The bracket of the electrode module was 3D printed using nylon. Nylon material has higher mechanical strength than normal resin material. Micro cylindrical polymer lithium batteries (55 mAh, 3.7 V) with the diameter and height of 8 and 14 mm, respectively, were used to power the self-powered wheel robot.

Superhydrophobic coating preparation: The nano-silica particles modified by the low surface energy polymer material were uniformly dispersed into the ethanol/butyl acetate mixed solvent by a mechanical dispersion process to form a uniform and stable nano-dispersion liquid. The solid content is controlled at 3-5%. The nano-dispersion liquid was sprayed on the surface of the plastic plate using a spray gun, and after the solvent is volatilized, a superhydrophobic surface on the plastic plate was formed.

Supporting Information

Supporting Information is available from the Wiley Online Library.

Acknowledgements

This research is partially supported by the National Natural Science Foundation of China (No. 51375468, 61503270). Dr. Shi-Yang Tang is the recipient of the Vice-Chancellor's Postdoctoral Research Fellowship funded by the University of Wollongong.

References

[1] a) W. Hu, G. Z. Lum, M. Mastrangeli, M. Sitti, *Nature* **2018**, *554*, 81; b) R. H. Armour, J. F. V. Vincent, *J Bionic Eng.* **2006**, *3*, 195-208; c) L. Van Griethuijsen, B. Trimmer, *Biol. Rev.* **2014**, *89*, 656-670.

[2] a) H. T. Lin, G. G. Leisk, B. Trimmer, *Bioinspir. Biomim.* **2011**, *6*, 026007; b) A. E. Hartl, A. P. Mazzoleni, *J. Spacecr. Rockets* **2010**, *47*, 493-502; c) N. Tan, R. E. Mohan, K. Elangovan, *Int. J. Adv. Robot Syst.* **2016**, *13*, 1729881416658180.

[3] a) K. Ilin, H. Moffatt, V. Vladimirov, *Proc. Natl. Acad. Sci. U. S. A.* **2017**, 201713685; b) W.-H. Chen, C.-P. Chen, J.-S. Tsai, J. Yang, P.-C. Lin, *Mech. Mach. Theory* **2013**, *68*, 35-48; c) V. A. Joshi, R. N. Banavar, R. Hippalgaonkar, *Mech. Mach. Theory* **2010**, *45*, 130-136; d) J. Park, S. Jung, *Mechatronics* **2013**, *23*, 594-606.

[4] a) E. Kayacan, Z. Y. Bayraktaroglu, W. Saeys, *Robotica* **2012**, *30*, 671-680; b) M. Zheng, Z. Qiang, L. Jinkun, C. Yao, *Chin. J. Aeronaut.* **2011**, *24*, 337-345; c) Y. Cai, Q. Zhan, X. Xi, *Mech. Mach. Theory* **2012**, *51*, 58-73; d) E. Kayacan, E. Kayacan, H. Ramon, W. Saeys, *IEEE T. Cybernetics* **2013**, *43*, 170-179.

[5] a) R. Chase, A. Pandya, *Robotics* **2012**, *1*, 3-23; b) S. Mahboubi, M. M. S. Fakhrabadi, A. Ghanbari, *J Intell. Robot Syst.* **2013**, *71*, 43-64; c) T. Umedachi, V. Vikas, B. Trimmer, *Bioinspir. Biomim.* **2016**, *11*, 025001.

[6] a) M. D. Dickey, R. C. Chiechi, R. J. Larsen, E. A. Weiss, D. A. Weitz, G. M. Whitesides, *Adv. Funct. Mater.* **2008**, *18*, 1097-1104; b) T. Liu, P. Sen, C.-J. Kim, *J. Microelectromech. Syst.* **2012**, *21*, 443-450; c) M. D. Bartlett, N. Kazem, M. J. Powell-Palm, X. Huang, W. Sun, J. A. Malen, C. Majidi, *Proc. Natl. Acad. Sci. U. S. A.* **2017**, *114*, 2143-2148; d) M. D. Bartlett, A. Fassler, N. Kazem, E. J. Markvicka, P. Mandal, C. Majidi, *Adv. Mater.* **2016**, *28*, 3726-3731.

[7] K.-Q. Ma, J. Liu, *J. Phys. D: Appl. Phys.* **2007**, *40*, 4722.

[8] a) C. Ladd, J. H. So, J. Muth, M. D. Dickey, *Adv. Mater.* **2013**, *25*, 5081-5085; b) J. W. Boley, E.

L. White, G. T. C. Chiu, R. K. Kramer, *Adv. Funct. Mater.* **2014**, *24*, 3501-3507; c) I. D. Joshipura, H. R. Ayers, C. Majidi, M. D. Dickey, *J. Mater. Chem. C* **2015**, *3*, 3834-3841; d) A. Fassler, C. Majidi, *Lab Chip* **2013**, *13*, 4442-4450.

[9] a) S. Ghosh, S. Lim, *Sci. Rep.* **2018**, *8*, 10169; b) B. J. Carey, J. Z. Ou, R. M. Clark, K. J. Berean, A. Zavabeti, A. S. Chesman, S. P. Russo, D. W. Lau, Z.-Q. Xu, Q. Bao, O. Kavehei, B. C. Gibson, M. D. Dickey, R. B. Kaner, T. Daeneke, K. Kalantar-Zadeh, *Nat. Commun.* **2017**, *8*, 14482; c) A. Zavabeti, J. Z. Ou, B. J. Carey, N. Syed, R. Orrell-Trigg, E. L. Mayes, C. Xu, O. Kavehei, A. P. O'mullane, R. B. Kaner, K. Kalantar-Zadeh, T. Daeneke, *Science* **2017**, *358*, 332-335; d) E. J. Markvicka, M. D. Bartlett, X. Huang, C. Majidi, *Nat. Mater.* **2018**, *17*, 618-624.

[10] a) J. Jeon, J. B. Lee, S. K. Chung, D. Kim, *Lab Chip* **2016**, *17*, 128-133; b) C. B. Eaker, M. D. Dickey, *Applied Physics Reviews* **2016**, *3*, 031103; c) J. Zhang, Y. Yao, L. Sheng, J. Liu, *Adv. Mater.* **2015**, *27*, 2648-2655.

[11] a) K. Khoshmanesh, S.-Y. Tang, J. Y. Zhu, S. Schaefer, A. Mitchell, K. Kalantar-Zadeh, M. D. Dickey, *Lab Chip* **2017**, *17*, 974-993; b) S.-Y. Tang, Y. Lin, I. D. Joshipura, K. Khoshmanesh, M. D. Dickey, *Lab Chip* **2015**, *15*, 3905-3911.

[12] Y. y. Yao, J. Liu, *RSC Adv.* **2016**, *6*, 56482-56488.

[13] S.-Y. Tang, V. Sivan, K. Khoshmanesh, A. P. O'Mullane, X. Tang, B. Gol, N. Eshtiaghi, F. Lieder, P. Petersen, A. Mitchell, K. Kalantar-zadeh, *Nanoscale* **2013**, *5*, 5949-5957.

[14] a) Y.-y. Yao, J. Liu, *RSC Adv.* **2017**, *7*, 11049-11056; b) S.-Y. Tang, K. Khoshmanesh, V. Sivan, P. Petersen, A. P. O'Mullane, D. Abbott, A. Mitchell, K. Kalantar-zadeh, *Proc. Natl. Acad. Sci. U. S. A.* **2014**, *111*, 3304-3309; c) S.-Y. Tang, V. Sivan, P. Petersen, W. Zhang, P. D. Morrison, K. Kalantar-zadeh, A. Mitchell, K. Khoshmanesh, *Adv. Funct. Mater.* **2014**, *24*, 5851-5858.

[15] M. R. Khan, C. B. Eaker, E. F. Bowden, M. D. Dickey, *Proc. Natl. Acad. Sci. U. S. A.* **2014**, *111*, 14047-14051.

[16] a) P. Mojabi, *J. Dyn. Syst. Meas. Control* **2004**, *126*, 678-683; b) E. D. Ferreira, S.-J. Tsai, C. J.

Paredis, H. B. Brown, *Adv. Robotics* **2000**, *14*, 459-475; c) F. Michaud, J.-F. Laplante, H. Larouche, A. Duquette, S. Caron, D. Létourneau, P. Masson, *IEEE Trans. Syst., Man, Cybern. A, Syst., Humans* **2005**, *35*, 471-480; d) Y. Sugiyama, A. Shiotsu, M. Yamanaka, S. Hirai. Circular/spherical robots for crawling and jumping; *Proceedings of the 2005 IEEE International Conference on Robotics and Automation* **2005**, 3595-3600.